Microwave Frequency Multiplier

Jose E. Velazco*

ABSTRACT. — High-power microwave radiation is used in the Deep Space Network (DSN) and Goldstone Solar System Radar (GSSR) for uplink communications with spacecraft and for monitoring asteroids and space debris, respectively. Intense X-band (7.1–8.6 GHz) microwave signals are produced for these applications via klystron and traveling-wave microwave vacuum tubes. In order to achieve higher data rate communications with spacecraft, the DSN is planning to gradually furnish several of its deep space stations with uplink systems that employ Ka-band (34-GHz) radiation. Also, the next generation of planetary radar, such as Ka-Band Objects Observation and Monitoring (KaBOOM), is considering frequencies in the Ka-band range (34–36 GHz) in order to achieve higher target resolution. Current commercial Ka-band sources are limited to power levels that range from hundreds of watts up to a kilowatt and, at the high-power end, tend to suffer from poor reliability. In either case, there is a clear need for stable Ka-band sources that can produce kilowatts of power with high reliability. In this article, we present a new concept for high-power, high-frequency generation (including Ka-band) that we refer to as the microwave frequency multiplier (MFM). The MFM is a two-cavity vacuum tube concept where low-frequency (2–8 GHz) power is fed into the input cavity to modulate and accelerate an electron beam. In the second cavity, the modulated electron beam excites and amplifies high-power microwaves at a frequency that is a multiple integer of the input cavity's frequency. Frequency multiplication factors in the 4 to 10 range are being considered for the current application, although higher multiplication factors are feasible. This novel beam-wave interaction allows the MFM to produce high-power, high-frequency radiation with high efficiency. A key feature of the MFM is that it uses significantly larger cavities than its klystron counterparts, thus greatly reducing power density and arcing concerns. We present a theoretical analysis for the beam-wave interactions in the MFM's input and output cavities. We show the conditions required for successful frequency multiplication inside the output cavity. Computer simulations using the plasma physics code MAGIC show that 100 kW of Ka-band (32-GHz) output power can be produced using an 80-kW X-band (8-GHz) signal at the MFM's input. The associated MFM efficiency — from beam power to Ka-band power — is 83 percent. Thus, the overall klystron-MFM efficiency is 42 percent — assuming that a klystron with an efficiency of 50 percent delivers the input signal.

* Communications Ground Systems Section.

The research described in this publication was carried out by the Jet Propulsion Laboratory, California Institute of Technology, under a contract with the National Aeronautics and Space Administration.

I. Introduction

Solid-state power amplifiers have made tremendous strides towards producing high-power microwave radiation and state-of-the-art devices can now produce tens of watts of power per unit. For instance, TriQuint offers gallium nitride (GaN) transistor chips that produce 100 W at X-band (model TGM2635-CP) and up to 9 W of power at Ka-band (model TGA2595).[1] For the case of monolithic microwave integrated circuit (MMIC) amplifiers based on advanced semiconductor technology such as GaN, higher power operation is limited by hotspots that occur on the semiconductor substrates. High-power densities along the traces on the device result in the generation of these hotspots, which can ultimately lead to the destruction of the device. Consequently, vacuum tubes remain as the only option for high-power microwave generation. High-power microwave radiation is typically achieved using tube amplifiers such as klystrons and traveling-wave tubes (TWTs). At Ka-band, state-of-the-art klystrons produce 2 kW of power,[2] while TWTs can deliver up to 200 watts.[3]

Klystrons and TWTs are vacuum devices that are based on beam-wave interactions between electrons and electromagnetic signals. An electron beam, focused by an external magnetic field, travels along the axis of these devices and interacts with the electromagnetic fields to be amplified. In the case of klystrons, a set of microwave cavity resonators is arranged in tandem and used to velocity-modulate a continuous electron beam into a bunched beam. An output cavity is used to extract power from the bunched beam and convert it into high-power microwaves. In the case of TWTs, a magnetically focused electron beam travels inside a helical conductor that carries a traveling electromagnetic wave. The pitch of the helix is such that the beam and wave undergo a continuous interaction as they move along the helix, gradually producing electron bunching. The bunched beam provides energy to the wave as it travels, creating a growing space-charge wave, thus producing microwave power amplification. In both cases, the radio frequency (RF) structures become smaller as the frequency is increased and beam interception by the tube body becomes an issue. Electron interception produces thermal heating of the tube body, which may result in tube failure. In addition, due to the high-power densities generated in the increasingly smaller structures, arcing and RF breakdown also becomes an issue.

Currently only one Deep Space Network (DSN) station is furnished with Ka-band uplink capability, where the output of two 200-W TWT amplifiers is combined using a two-way waveguide power combiner to produce a total of 300 W Ka-band output power (100 W are lost along the power combining circuit). The DSN is planning to expand its Ka-band capabilities at least to two other stations and is looking at several options, including solid-state arrays and vacuum tubes. Ka-Band Objects Observation and Monitoring (KaBOOM)[4] is also considering employing vacuum tubes for their radar transmitters to fulfill its need for multi-kilowatt Ka-band radiated power.

---

[1] http://www.triquint.com/products/all/amplifiers/high-power-amplifiers

[2] http://www.cpii.com/docs/datasheets/44/VKA-7934.pdf

[3] http://www2.l-3com.com/eti/downloads/ka_quad.pdf

[4] https://www.nasa.gov/directorates/heo/scan/engineering/technology/KaBOOM.html

The microwave frequency multiplier (MFM) presented here is a new concept for the generation of high-power, high-frequency electromagnetic radiation. The MFM concept is an alternative to klystrons and traveling-wave tubes. It should allow the generation of high-frequency electromagnetic power (including Ka-band) while avoiding RF breakdown and destructive thermal issues common to its tube counterparts. It consists of (see Figure 1) an input cavity, an output cavity, a magnetic focusing system, and an electron beam. Both the input and output cavities are cylindrically shaped. The input cavity operates in a transverse magnetic (TM) rotating-wave mode at a frequency ω while the output cavity works at a frequency $m\omega$, where m is a multiple integer greater than 1. When a high-power signal, operating at ω, is injected into the input cavity, it sets rotating-wave fields inside that oscillate at ω and that rotate azimuthally about the cavity axis at ω [1,2]. As it traverses the cavity, the electron beam is coherently modulated by the cavity rotating-wave fields and is gradually accelerated to high energies. The accelerated electrons are subsequently injected into the output cavity where they generate and interact with rotating-wave fields that operate at $m\omega$. During the output cavity interaction, the electrons give up a large amount of their power to the cavity fields, thus generating high power radiation at m times the input frequency. The beam-wave interaction in the output cavity is synchronous and therefore highly efficient. High efficiency results from the fact that the electrons remain phase-locked to the cavity fields, thus transferring most of their power to the fields.

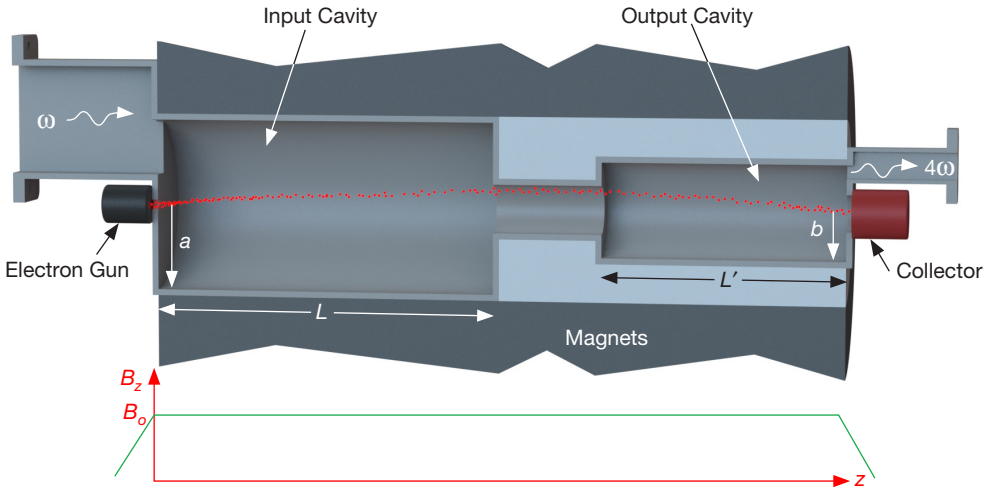

Figure 1. Schematic showing the proposed microwave frequency multiplier.

It should be noted that the MFM requires a high-power, low-frequency signal at the input. Most of the input RF power is added to the electron beam during beam acceleration along the input cavity. In the output cavity, the beam power is synchronously transferred to the output fields. Thus, the MFM is basically a device that converts the high-power, low-frequency input signal into a higher frequency signal with similar power levels.

In this article, we first provide a simple linear theory of the acceleration process in the MFM input cavity [3,4]. Subsequently, we present analysis of the beam-wave interaction along the output cavity. Conditions are presented under which continuous power transfer from

the beam to the output cavity fields is achieved. We also present computer simulations obtained in the particle-in-cell code MAGIC[5] to optimize the beam acceleration process. We conclude with calculations that show overall efficiency for a Ka-band MFM.

II. Accelerator Cavity Resonator

The MFM uses an input cavity accelerator to modulate the electron beam for optimum frequency multiplication in the output cavity. The electrons and fields undergo a synchronous interaction where the fields gradually add energy to the beam. Intensive studies of synchronous beam-wave interactions have been carried out by the authors of this article in related works[6] [5,6,7,8]. In the mechanism proposed herein, beam acceleration is obtained in a TM_{110} rotating-mode cylindrical resonator along with an axisymmetric magnetostatic focusing field. (The indices 1,1,0 indicate the wave periodicity in ϕ, r, and z, respectively.) To produce continuous beam acceleration, the static magnetic field along this cavity is adjusted such that the electron gyrofrequency is equal to the drive frequency. Under this gyroresonant condition, the beam electrons will undergo acceleration, maintaining strong temporal coherence with the RF rotating mode. The intensity of the RF field inside the cavity is adjusted such that the beam is coherently accelerated to the required beam energy level.

Let us assume a small-diameter beam moving along an axisymmetric static magnetic field $B = \hat{z}B_o$ with a velocity $\nu = \hat{x}\nu_x + \hat{y}\nu_y + \hat{z}\nu_z$ (see Figure 1). The motion of the beam-centroid inside a TM_{110} rotating-mode cavity is governed by the general equation

$$\frac{d}{dt}(m_o\gamma\nu) = -|e|\left[\tilde{E} + \nu \times \tilde{B} - B_o\nu \times \hat{z}\right] \tag{1}$$

where $\tilde{E}$ and $\tilde{B}$ are, respectively, the RF electric and magnetic fields present, B_o is the amplitude of the static magnetic field, and relativistic mass factor, γ, is the electron's energy normalized to its rest energy. The electrons' mass and charge are denoted by m_o and e, respectively. For a TM_{110} rotating-mode resonator, the complete set of equations, in cylindrical coordinates (r,ϕ,z) is given by[7]

$$\tilde{E}(r,\phi,z;t) = \hat{z}2B_{rf}J_1\left(k_\perp r\right)\sin\left(\omega t - \phi\right) \tag{2}$$

$$\tilde{B}(r,\phi,z;t) = \hat{\phi}2B_{rf}J_1\left(k_\perp r\right)\sin\left(\omega t - \phi\right) + \hat{r}2B_{rf}\frac{1}{k_\phi r}J_1'\left(k_\perp r\right)\cos\left(\omega t - \phi\right) \tag{3}$$

where B_{rf} is a constant that describes the RF magnetic field amplitude near-axis, J_1 is the first-order Bessel function of the first kind, $k_\perp = u_{11}/a$ is the radial wave number, u_{11} is the first root of $J_1(u_{11}) = 0, J_1' = \frac{d}{dk_\perp r}[J_1(k_\perp r)]$, a is the cavity radius, and ω is the drive radial frequency, which for this mode is defined as

$$\omega = ck_\perp = \frac{u_{11}c}{a}. \tag{4}$$

---

[5] MAGIC User's Manual, Orbital ATK, Inc., Newington VA.

[6] J. E. Velazco, "The Study of Synchronous Beam-Wave Interactions for the Generation of Coherent Microwave Radiation," PhD Dissertation, George Mason University, 1994.

[7] Ibid.

The RF field equations (Equations 2 and 3) present no axial coordinate dependence and thus are the same at any z-plane along the cavity length. Also, inspection of the phase argument of these fields $\omega t - \phi$ allows the easy derivation of the azimuthal velocity of the fields, $\Omega_{rot} \equiv d\phi/dt = \omega$.[8] Consequently, in this mode the fields resonate and rotate azimuthally at ω, i.e., they perform one gyration about the cavity axis in one RF period. The field lines for the electric and magnetic fields of the TM_{110} mode are shown in Figure 2.

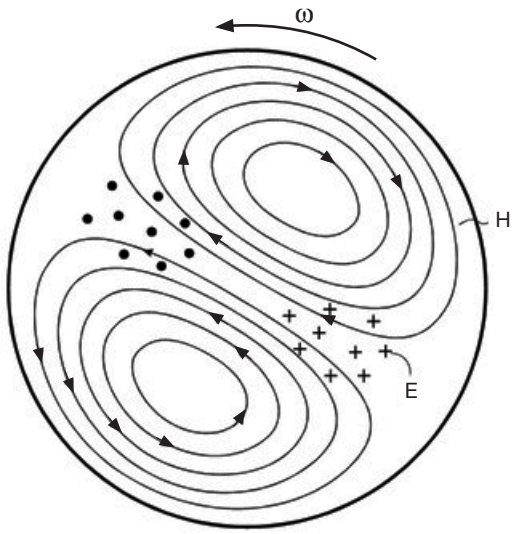

Figure 2. Field lines of electric and magnetic fields in TM_{110} rotating mode.

The input cavity beam-wave interaction occurs near axis where the argument $k_\perp r \leqslant 1$. The field equations (Equations 2 and 3) in the paraxial region, in rectangular coordinates (x,y,z), can thus be reduced to

$$\tilde{E}(x,y,t) = \frac{B_{rf}}{\omega}\left[x\cos(\omega t) + y\sin(\omega t)\right]\hat{z} \tag{5}$$

$$\tilde{B}(x,y,t) = B_{rf}\left[\hat{x}\cos(\omega t) + \hat{y}\sin(\omega t)\right]. \tag{6}$$

The TM_{110} rotating mode presents a constant magnetic field on-axis, and an electric field that approaches zero on-axis but that, off-axis, grows linearly with the values of the x–y coordinates.

Next, we calculate the equations of motion of the electron beam as it moves inside the input cavity under the influence of the rotating-mode TM_{110} fields and the static magnetic field.

To solve the general equation of motion of the beam, we assume that the fields inside the cavity are small. This allows us to consider the axial velocity and relativistic mass factor to be a constant. The beam is injected into the cavity at $t = t_o$ and exits the cavity at $t = t_o + \tau$, where τ is the electron's transit time along the cavity. Defining the transverse velocity and transverse displacement of the beam as $\nu_\perp \equiv \nu_x + i\nu_y$ and $\zeta_\perp \equiv x + iy$, respectively, the

[8] Ibid.

solution of Equation (1) for a beam entering the cavity at the injection time t_o yields the following equations of motion:

$$\nu_\perp(x,y,t) = \frac{-\nu_z \Omega_{rf}}{\omega} \cdot \exp(i\omega t_o) \cdot \left\{ \frac{1}{\left[\frac{\Omega_c}{\omega} - 1\right]} \cdot \exp(i\omega\tau) \left\{ \exp\left[i\omega(\Omega_c/\omega - 1)\tau\right] - 1 \right\} \right\} \tag{7}$$

$$\zeta_\perp(x,y,t) = -i\frac{\nu_z \Omega_{rf}}{\omega^2} \exp(i\omega t_o) \cdot \left\{ \frac{1}{\left[\frac{\Omega_c}{\omega} - 1\right]} \cdot \left[\exp(i\omega\tau) \left\{ \frac{\omega}{\Omega_c} \exp\left[i\omega(\Omega_c/\omega - 1)\tau\right] - 1 \right\} - \frac{\omega}{\Omega_c} + 1 \right] \right\} \tag{8}$$

where $\Omega_c = eB_o/m_o\gamma_o$ is the relativistic gyrofrequency of the electrons, $\Omega_{rf} = eB_{rf}/m_o\gamma_o, \nu_z$ is the beam's axial velocity, here assumed constant, and γ_o is the relativistic factor at $t = t_o$.

To calculate the change in beam energy γmc^2 as it traverses the cavity under a varying magnetic field (Ω_c), we shall use the unperturbed electron orbits given by Equation 8. For a single particle moving with a constant velocity, ν_z, the rate of change in the particle's energy can be calculated as follows:

$$\frac{d}{dt}\left(\gamma mc^2\right) = -|e|\nu_z E_z. \tag{9}$$

The value of the electrons' energy $\gamma(t)$ at any time t during this interaction is calculated by replacing Equations 5 and 8 in Equation 9 and solving as

$$\gamma(t) = \gamma_o \left[1 - \beta_z^2 \left(\frac{\Omega_{rf}}{\Omega_c} \right)^2 \times \psi \frac{\Omega_c}{\omega} \right] \tag{10}$$

where $\beta_z = v_z/c$ and $\psi(\Omega_c/\omega)$ is a frequency factor defined as

$$\psi\left(\frac{\Omega_c}{\omega}\right) = \frac{\Omega_c}{\omega} \times \frac{1}{\left(\frac{\Omega_c}{\omega} - 1\right)} \times \left[\frac{1}{\left(\frac{\Omega_c}{\omega}\right) - 1} \times \left\{ \cos\left[\omega\tau\left(\frac{\Omega_c}{\omega} - 1\right)\right] - 1 \right\} + \left(1 - \frac{\Omega_c}{\omega}\right) \times \left[\cos\omega\tau - 1\right] \right]. \tag{11}$$

Figure 3 illustrates the frequency factor as a function of interaction time of the beam in the "accelerator" resonator for different conditions of $\frac{\Omega_c}{\omega}$. It can be observed that under the gyroresonant condition $\Omega_c = \omega$, the beam gradually extracts energy from the RF fields of the input resonator and consequently undergoes acceleration as it is coherently spun-up by the rotating RF fields.

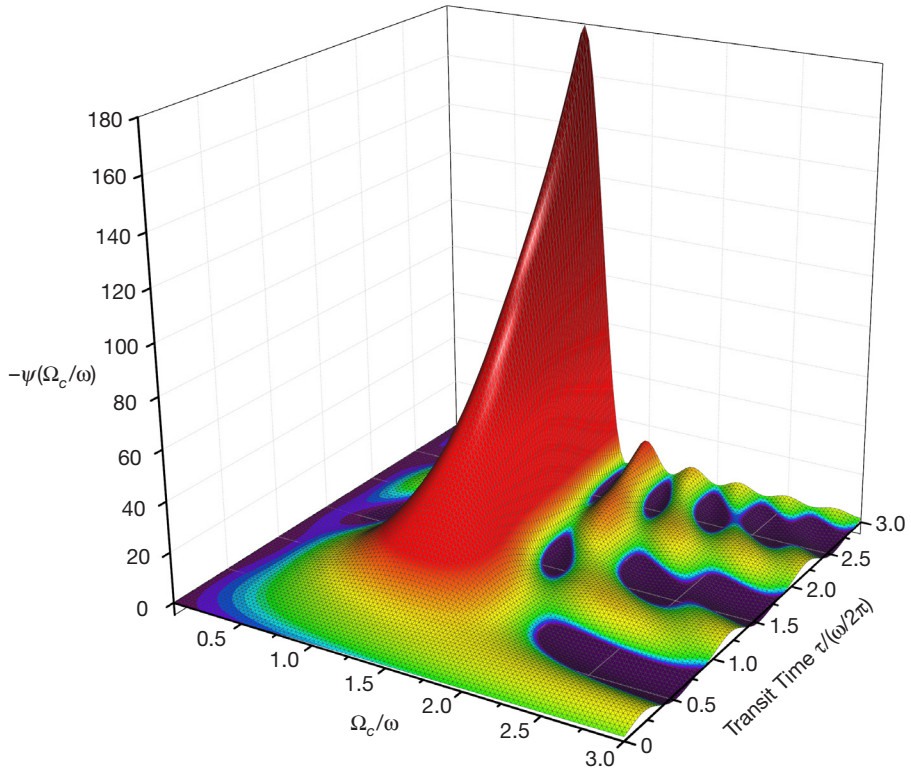

Figure 3. Plot of frequency factor, $\psi(\Omega_c/\omega)$, as a function of interaction time τ and Ω_c/ω ratio.

Assuming an interaction time inside the accelerator cavity that is a multiple integer of the RF period, e.g., $\tau = l \cdot 2\pi/\omega$, where $l = 1, 2, 3\ldots$, Equations 7 and 8 reduce to

$$\nu_{\perp}(x,y,\tau) = i\frac{\nu_z \Omega_{rf}}{\omega} \cdot [2\pi l] \cdot \exp(i\omega t_o) \tag{12}$$

$$\xi_{\perp}(x,y,\tau) = -\frac{\nu_z \Omega_{rf}}{\omega^2} \cdot [2\pi l] \cdot \exp(i\omega t_o) \tag{13}$$

Equations 7 and 8 can be further reduced, by assuming $\nu_t = i\frac{\nu_z \Omega_{rf}}{\omega} \cdot [2\pi l]$, to

$$\nu_{\perp}(x,y,\tau) = \nu_t \cdot \exp(i\omega t_o) \tag{14}$$

$$\xi_{\perp}(x,y,\tau) = i\frac{\nu_t}{\omega} \cdot \exp(i\omega t_o) \tag{15}$$

Equations 14 and 15 simply describe the motion of an electron under the presence of a static magnetic field. The electron gyromotion occurs with a velocity ν_t and with a gyrating radius ν_t/ω. The value of the electrons' transverse velocity is dictated by the intensity of the RF fields inside the accelerator cavity (Ω_{rf} or B_{rf}).

The electrons' energy after acceleration, from Equation 10, is given by

$$\gamma(\tau) = \gamma_o \left[1 + \beta_z^2 \left(\frac{\Omega_{rf}}{\Omega_c}\right)^2 \times \psi(1)\right]. \tag{16}$$

A. Input RF Power

We have also calculated the amount of microwave power necessary to produce beam acceleration to the desired electron energy. For a cylindrical cavity of radius a and length L, working at a frequency ω, the input power is given as

$$P_i = P_L + P_b \tag{17}$$

where P_L is the power lost to the cavity walls, defined as

$$P_L = \frac{R_s \pi}{Z_o^2}\left[caJ_o\left(k_\perp a\right)\right]^2 B_{rf}^2 \left(\frac{L}{a}+1\right) \tag{18}$$

and P_b is the amount of power absorbed by the beam, given by

$$P_b = I_o V_f \tag{19}$$

where R_s is the resistivity of the cavity walls in ohms, $Z_o = 377$ ohms is the intrinsic impedance of free space, J_o is the zeroth-order Bessel function of the first kind, V_f is the final energy of the beam, and I_o is the beam current. For example, in order to accelerate a 50-kV, 1-A beam to a final energy of 120 keV (at 1 A), the required average input power for a copper cavity operating with at 8 GHz would be 80 kW. From the required 80 W, the cavity walls will dissipate a small portion of the required power (10 kW), whereas 70 kW will be added to the beam.

III. Drift Region Dynamics

In this section, we assume that the electrons have been circularly scanned by the accelerator resonator. Solution of the beam's equations of motion for the drift region yields

$$\nu(z,t) = \nu_t \exp\left\{i\left[\omega t + \left(\Omega_c' - \omega\right)\frac{z}{\nu_z}\right]\right\} \tag{20}$$

$$\xi_\perp(z,t) = i\frac{\nu_t}{\Omega_c'}\exp\left\{i\left[\omega t + \left(\Omega_c' - \omega\right)\frac{z}{\nu_z}\right]\right\} \tag{21}$$

where Ω_c' is the cyclotron frequency in the drift region, ν_t is the transverse velocity of the beam, and t is the time along this region. At this point, it is important to characterize the beam dynamics in this region. Equations 20 and 21 represent the dynamics of an electron performing gyromotion about the lines of a static magnetic field at an angular velocity ω with a gyration radius ν_t/Ω_c'. Thus, in the drift region the beam streams along the z direction describing a spiral in space, with a pitch given by $(\Omega_c' - \omega)/\nu_z$. It should also be pointed out that each electron conforming to the spiral will gyrate about the device axis at the drive frequency and with a gyration radius R_g equal to the radius of the spiral, $R_g = \nu_t/\Omega_c'$. The projection of the beam orbits in this region onto the transverse plane will be a ring whose thickness is equal to the initial beam diameter.

Next we analyze the beam-wave interactions between a modulated e-beam described by Equations 20 and 21 and the fields of a TM_{m10} mode. (The indices m, 1, 0, indicate the wave periodicity in ϕ, r, and z, respectively.)

IV. Output Cavity Dynamics

In order to evaluate the conditions for optimum interaction between the modulated electron beam and fields of the output TM_{m10} mode, we shall assume that the magnetic field along the output cavity is not yet fixed so that the electron's cyclotron frequency along that region Ω_c' is defined as

$$\Omega_c' = eB_o'/m_o\gamma_a \tag{22}$$

where γ_a is the electron's relativistic mass factor after acceleration (given by Equation 16), and B_o' is the amplitude of the external magnetic field in this region. In addition, we shall assume that the entry conditions for the electron beam into the output cavity are given by Equations 20 and 21.

Hereafter, we derive expressions that describe the matching conditions required for efficient beam-wave energy transfer in the output cavity. The general expression for the transverse electric fields of a TM_{m10} guided circularly polarized electromagnetic wave in a cylindrical cavity of radius b, in cylindrical coordinates (r,ϕ,z), is given by [1]

$$E_z(r,\phi,t) = E_o J_m\left(k_\perp' r\right)\cos\left(\omega_o t - m\phi\right) \tag{23}$$

where E_o is the electric field amplitude, J_m is the m^{th} Bessel function of the first kind, and where the output frequency ω_o and wave number $k_\perp'$ are related by the guided wave dispersion relation

$$\omega_o = ck_\perp' \tag{24}$$

where c is the speed of light, $k_\perp' = u_{m1}b$, and u_{m1} is the m^{th} root of $J_m(u) = 0$.

Next, we seek an expression for the rate of energy transfer $P(z,t)$ from the spiraling beam to the fields of a TM_{m10} rotating mode. The index m depicts the azimuthal periodicity of the wave fields and can take values of $m = \pm 1, \pm 2, \pm 3, \pm 4\ldots$. We claimed in a related work [1,2] that in rotating modes of this type, the mode resonates at ω_o but its fields rotate about the cavity axis at ω_o/m. This feature, as will be shown later, permits the temporal synchronization of a rotating spiraling beam with the fields of a rotating mode operating at a frequency that is a higher harmonic m of the rotating frequency of the beam.

We shall henceforth consider a cold electron beam streaming along a uniform axisymmetric magnetostatic field carrying an axial current density J_{oz} characterized by

$$J_{oz}\left(r,\phi,z,t\right) = -|\,e\,|n_o A\nu_z\,\delta\left(x - R_g\cos\Theta\right)\cdot\delta\left(y - R_g\sin\Theta\right), \tag{25}$$

where n_o is the beam density, A its cross-sectional area, and $\Theta = \omega t + (\Omega_c' - \omega)z/\nu_z$ is the electron's gyrophase. For such a beam, the instantaneous rate of change of the particles' energy can be calculated as

$$P(z,t) = \int dz \int drr \int d\phi \boldsymbol{J}(r,\phi,z,t)\cdot\boldsymbol{E}(r,\phi,z,t) \tag{26}$$

where E is described by Equation 23 and where E_o is assumed to vary slowly relative to the electron transit time scale. It is also assumed that the beam's axial velocity remains constant during its transit through the cavity. Upon manipulation of the above equation for power transfer, the radiated power to the output cavity's fields can be expressed as

$$P(z,t) = I_o E_o J_m\left(k'_\perp R_g\right)L'\left\{\frac{(\sin[(\omega_o - m\omega)t - m(\Omega'_c - \omega)L'/\nu_z] - \sin[(\omega_o - m\omega)t])}{m(\Omega'_c - \omega)L'/\nu_z}\right\} \quad (27)$$

where $I_o = en_o\nu_z A$ is the beam's dc current and where L' is the length of the output cavity. The average output power, averaged over the interaction time τ_o, $\langle P_z\rangle = 1/\tau_o \int_o^{\tau_o} dtP_z(z,t)$ becomes

$$\langle P\rangle = I_o E_o J_m\left(k'_\perp R_g\right)L' \cdot\left\{\frac{\left(\cos\left[m(\Omega'_c - \omega)L'/\nu_z - (\omega_o - m\omega)\tau_o\right] - \cos\left[m(\Omega'_c - \omega)L'/\nu_z\right] - \cos\left[(\omega_o - m\omega)\tau\right]\right) + 1}{m(\Omega'_c - \omega)L'/\nu_z \times (\omega_o - m\omega)\tau_o}\right\}. \quad (28)$$

At equilibrium, the power dissipated by the cavity should equal the power radiated by the beam. The power dissipated by the cavity can be expressed as

$$\langle P\rangle = \frac{\omega_o}{Q_L}U \quad (29)$$

where Q_L is the cavity-loaded Q. The stored energy inside the output cavity, U, can be calculated as $U = \int\int\int \frac{\varepsilon}{2}|E_z|^2 d\phi r dr dz$, which, after solving, yields

$$U = \frac{1}{2}\pi\varepsilon b^2 L' J'^2_m(k'_\perp b)E_o^2. \quad (30)$$

Next, by equating Equations 28 and 29, an expression for the electric field E_o can be found, which can be replaced back into Equation 28 to yield an expression for the output power as

$$P_o = I_o^2 Z_o Q_L\left(\frac{2}{\pi}\right)\left(\frac{L'}{b}\right)C_m S_m \quad (31)$$

where $Z_o = \sqrt{\mu/\varepsilon}$ is the free-space wave impedance. Here, C_m is introduced to denote the coupling strength between the beam electrons and the RF electric rotating wave field defined as

$$C_m = \left\{\left(\frac{1}{u_{mn}}\right)\left[\frac{J_m(u_{mn}R_g/b)}{J'_m(u_{mn})}\right]^2\right\}. \quad (32)$$

S_m is a synchronism factor that contains the information of the beam-wave temporal matching, and is given by

$$S_m(\chi_1,\chi_2) = \left(\frac{\cos(\chi_1 - \chi_2) - \cos\chi_2 - \cos\chi_1 + 1}{\chi_1\chi_2}\right)^2, \quad (33)$$

where $\chi_1 = (\omega_o - m\omega)$ and $\chi_2 = m(\Omega_c' - \omega)L'/\nu_z$. The synchronism factor S_m is plotted in Figure 4 as a function of χ_1 and χ_2, where it is seen to reach a maximum of unity for $\chi_1 = \chi_2 = 0$. For finite values of L' and τ_o, S_m is maximized when the synchronism conditions

$$\omega_o = m\omega, \tag{34a}$$

$$\Omega_c' = \omega, \tag{34b}$$

are satisfied. The synchronism condition states that maximum transfer of energy from the helical electron beam to the rotating fields of the TM mode is achieved when the entry point of the helical beam into the cavity rotates temporally about the axis at $1/m$ the RF output frequency and when the gyrofrequency of each single electron is equal to the drive frequency. Observance of these conditions should allow cumulative energy transfer from the beam to the fields of the cavity at very high efficiencies. Note also that the output power of this device grows quadratically with beam current and is linearly dependent on the cavity length. Thus, the cavity length can be freely adjusted for optimum energy extraction from the beam at the design mode.

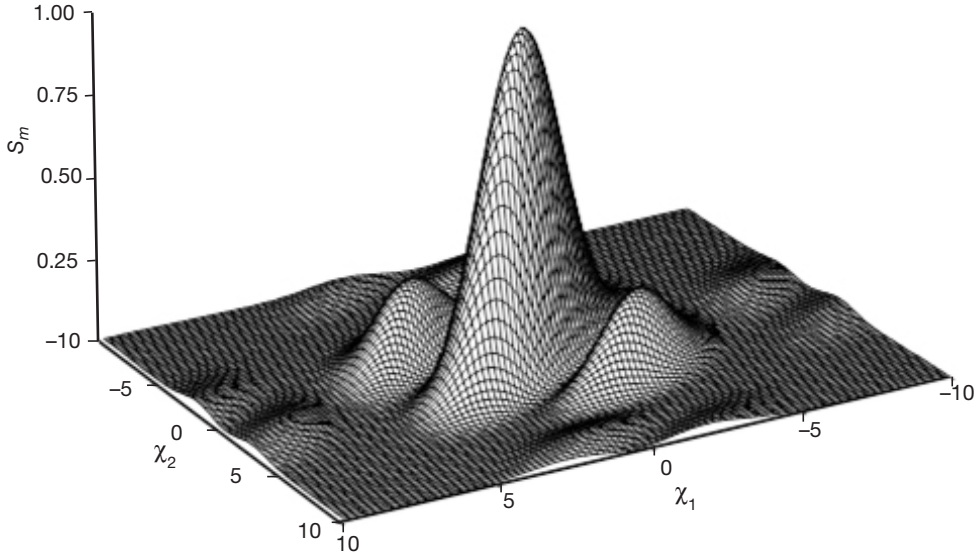

Figure 4. Three-dimensional plot of synchronism factor S_m as a function of χ_1 and χ_2.

To proceed, we shall assume that the synchronism conditions given by Equation 34 have been satisfied. Under these conditions, the normalized gyroradius is $R_g/b = m\beta_t/u_{mn}$, which can be plugged into Equation 32 to unveil the dependence of the coupling factor on β_t. (Here, we have introduced β_t, which is the transverse velocity normalized to the speed of light, i.e., $\beta_t = \nu_t/c$. Figure 5 illustrates plots of C_m as a function of β_t for different values of the azimuthal index m. The radial index n is set to 1. It can be observed that for a given m, the strength of the beam-wave coupling is increased as β_t increases.

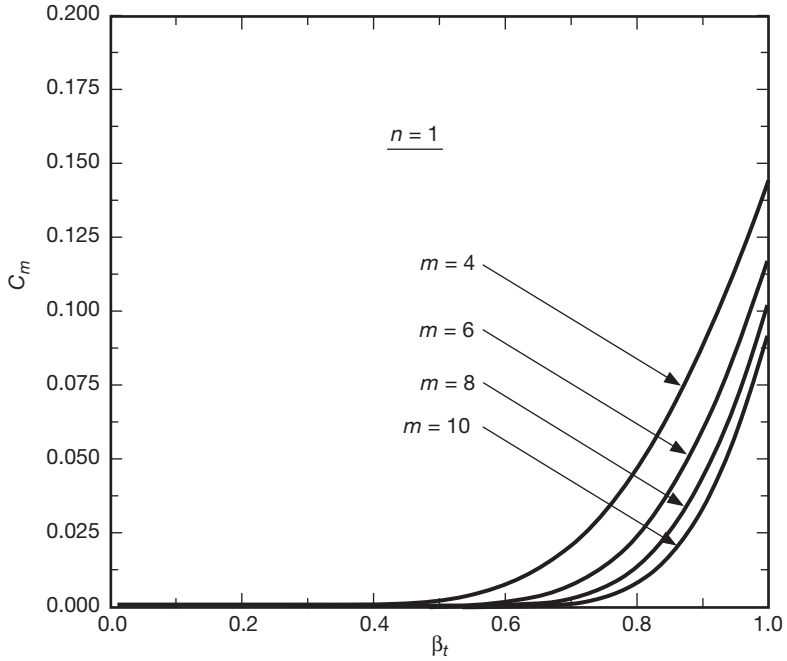

Figure 5. Plots of C_m as a function of β_t for different values of the azimuthal index *m*.

V. MAGIC Computer Simulation Results

In this section, we show results of three-dimensional nonlinear studies performed on the three-dimensional plasma physics particle-in-cell (PIC) fully self-consistent code MAGIC.[9] (MAGIC is a fully self-consistent, three-dimensional, time-dependent code that allows one to look at the time-evolution of the particle motion, nonlinear effects, and additional forces or conditions, which are not readily tractable by other methods.) The results of our linear theory were employed to determine the initial parameters for our numerical study and were not intended to be utilized for the prediction of nonlinear dynamics. Figure 6 illustrates typical MAGIC results for the input cavity. An electron beam with an initial energy of 50 keV and 1 A current is injected into a cylindrical cavity holding a rotating TM_{110} mode. A focusing magnetic field is applied and is adjusted to maintain gyroresonance. Figure 6(a) shows the energy of the electron beam as a function of interaction length. Electrons are gradually accelerated to a final energy of 140 keV at the end of the cavity. Figure 6(b) shows the beam trajectory as a function of interaction length for same cavity parameters.

Next we present results of MAGIC simulations performed for the MFM's output cavity. The results of our theory are employed to determine the initial parameters for our numerical study. In the simulations, a 120-keV, 1-A rotating beam, modulated at 8 GHz, is injected into an empty cylindrical cavity. The cavity radius is 1.1 cm and its length is selected for optimum beam-wave interaction. The selected cavity dimensions, according to Equation 24, should allow the excitation of the TM_{410} mode at four times the drive frequency, i.e., 32 GHz. Figure 7 illustrates a MAGIC plot of the beam energy and trajectory as a function of interaction length. Note from Figure 7(a) that at the end of the cavity, the beam energy goes from 140 keV to 50 keV, corresponding to an efficiency of 64 percent.

[9] MAGIC User's Manual, Orbital ATK, Inc., Newington VA.

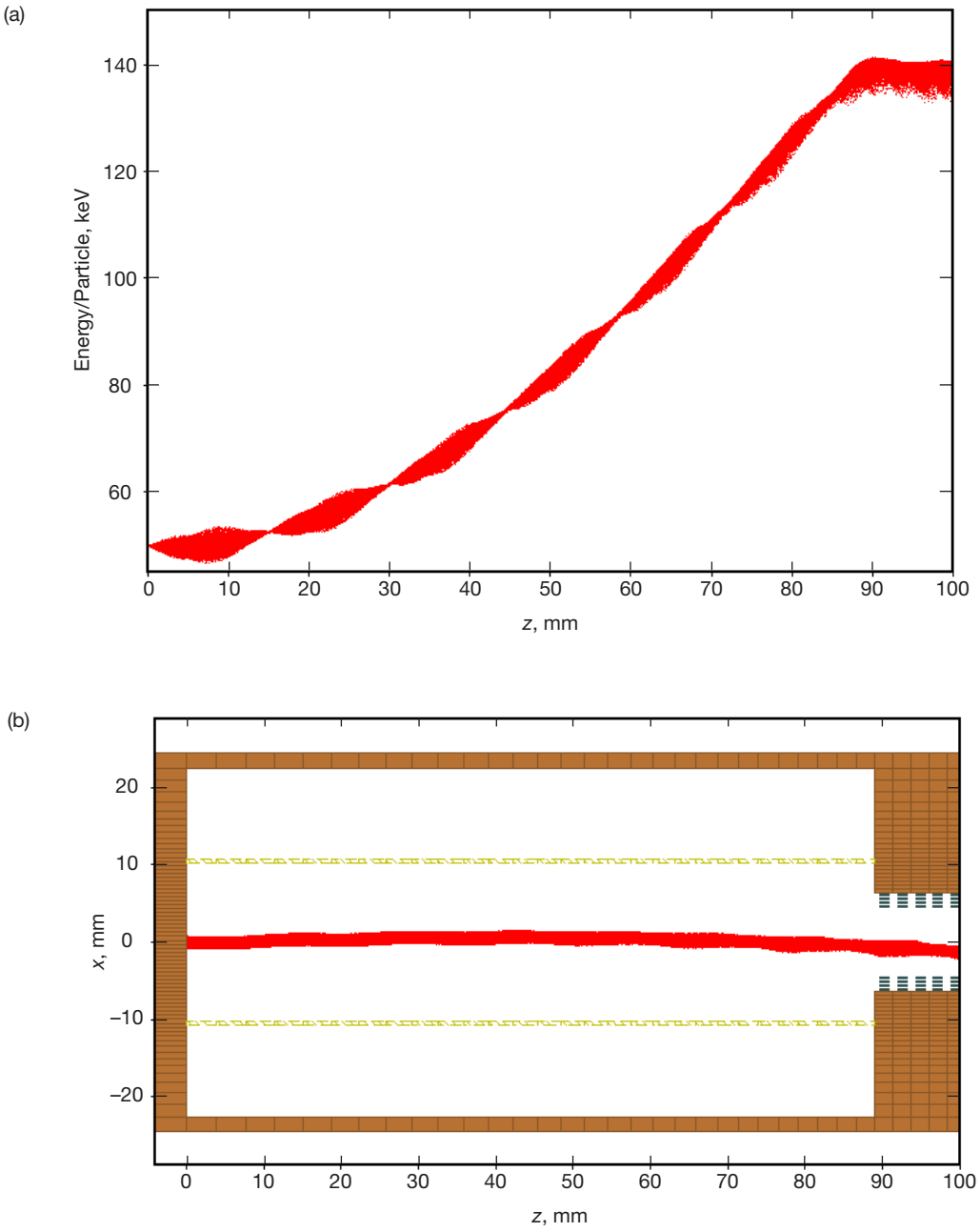

Figure 6. Electron beam dynamics along the accelerator resonator calculated on 3D PIC code MAGIC. (a) Beam energy and (b) beam trajectory are shown as a function of interaction length. The cavity radius is 2.2 cm. The cavity frequency is 8 GHz, initial beam voltage is 50 kV, and initial current is 1 A.

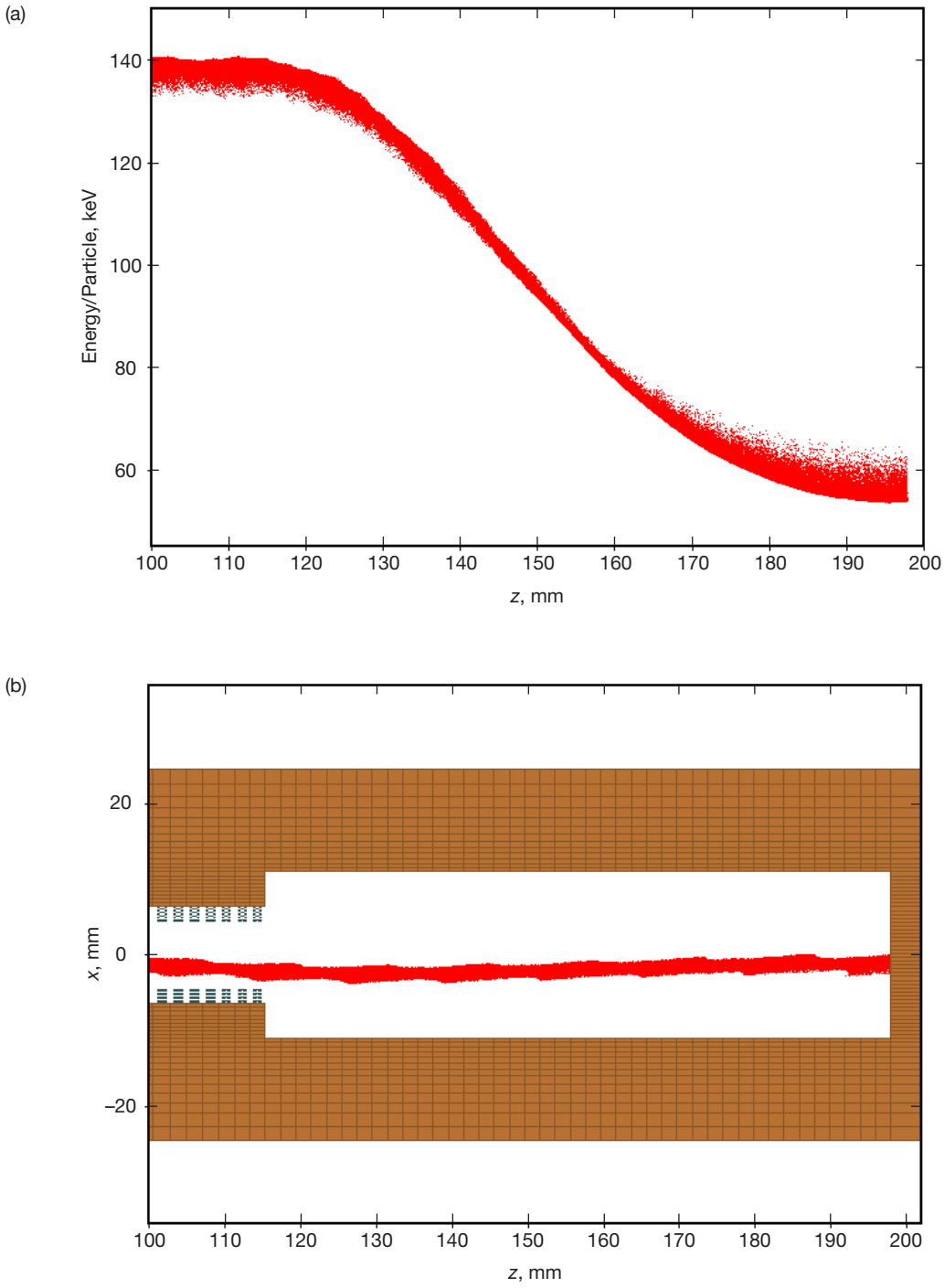

Figure 7. Beam dynamics along the output cavity. (a) Beam energy and (b) beam trajectory are shown as a function of interaction length (cavity radius is 1.1 cm). Other parameters are shown in the text.

Figure 8 shows plots of the RF electric field excited inside the cavity by the electron beam. Figure 8(a) shows the gradual increase of the electric field inside the cavity. The frequency spectrum of the RF electric field excited by the beam is shown in Figure 8(b). Note that single-mode excitation is achieved at 32 GHz.

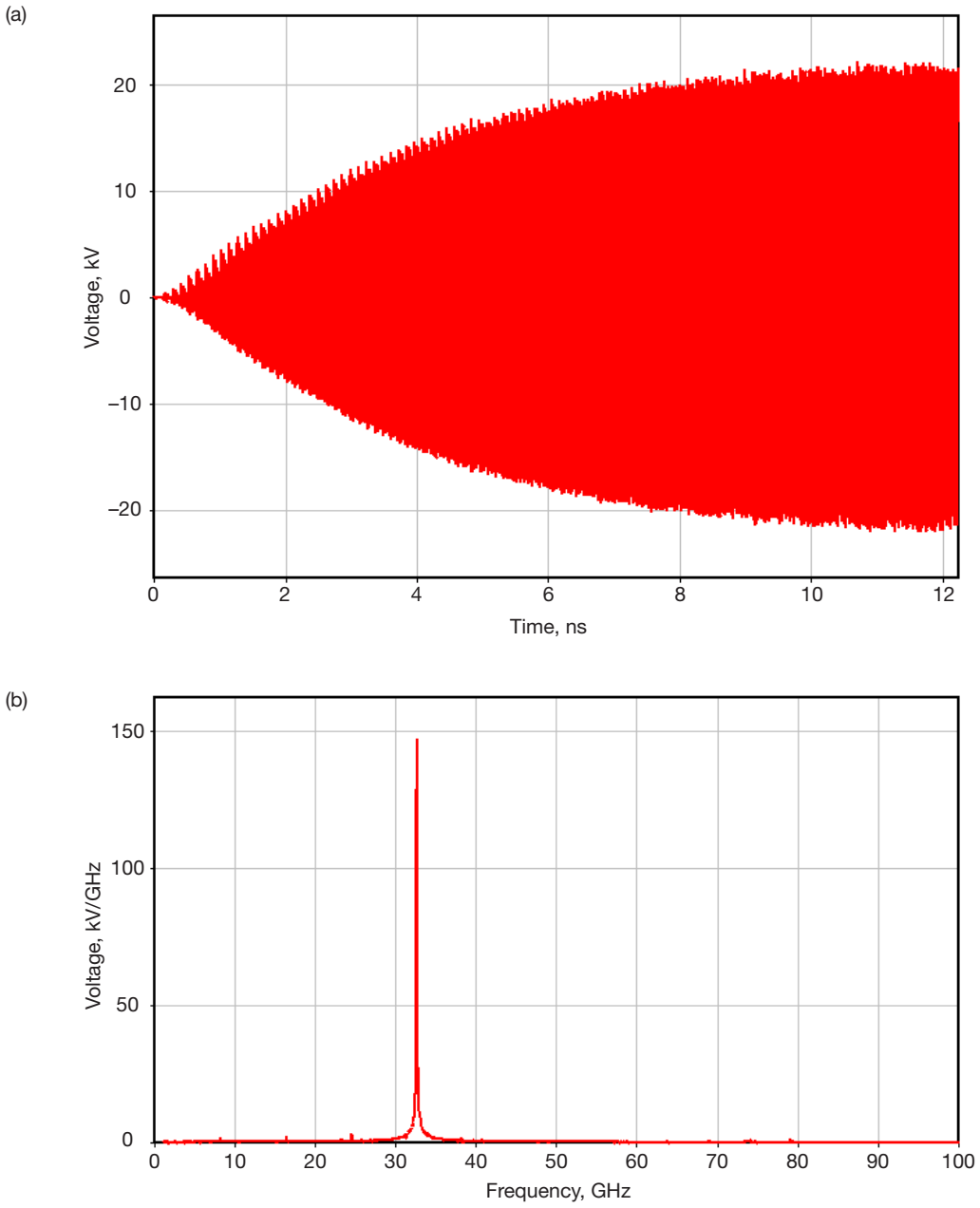

Figure 8. Results of MAGIC simulations of the output interaction. (a) RF voltage of the output mode and (b) frequency spectrum of electric field (RF voltage) are shown.

VI. System Efficiency and Gain

The overall system efficiency η_s can be calculated as

$$\eta_s = \frac{\eta_{RF}\eta_{klys}}{1-\eta_c\left(1-\eta_{RF}\right)}, \tag{35}$$

where η_{RF} is the RF conversion efficiency from beam power to RF power inside the MFM output cavity and η_{klys} is the efficiency of the klystron. We have also included the recovering efficiency of the depressed collector η_c. Typically, when the spent electron beam arriving to the collector is nearly monoenergetic, an energy recovery scheme, such as a depressed collector, is used. A depressed collector recovers the electron voltage and feeds it back to the electron gun power supply. In this way, the device efficiency is greatly improved. Note in Equation 35 that if no energy recovery scheme is utilized, $\eta_c = 0$, then the system efficiency is given by the product of the klystron and MFM efficiencies, $\eta_{RF} \cdot \eta_{klys}$. For example, for an X-band klystron efficiency of 50 percent and assuming an MFM efficiency of 83 percent plus $\eta_c = 60$ percent, we get $\eta_s = 46$ percent. If no depressed collector is employed, then the system efficiency is $\eta_s = 42$ percent.

The system gain can be expressed as

$$G_s\left(dB\right) = G_{klys}\left(dB\right) + G_{MFM}\left(dB\right), \tag{36}$$

where G_{klys} is the klystron's gain and G_{MFM} is the gain of the frequency multiplier. For a klystron gain of 50 dB and an MFM gain of 0 dB, we obtain a system gain of 50 dB.

VII. Point Design Parameters — 100-kW Ka-Band MFM

An example of a set of working parameters for this high-power frequency multiplier is shown in Table 1. The input power is assumed to be provided by an X-band klystron capable of delivering 80 kW at 8 GHz. A 50-kV, 1-A pencil beam, generated in a suitable high-convergence gun, is injected into the accelerator resonator. The magnitude of the initial focusing magnetostatic field is set to provide gyroresonance. The input power is coupled into the cavity through two X-band waveguides arranged 90 deg apart spatially and with an electronic shift of 90 deg also. This is done to launch the circularly polarized TM_{110} mode in the cavity. Our analysis predicts that for suitable values of B_{rf} and B_o, the final beam energy factor after acceleration is $\gamma_a = 1.235$, which corresponds to a beam energy of 120 keV. Under these conditions, the amount of RF power transferred to the beam, as it is accelerated, is 70 kW. Assuming an 87 percent conversion efficiency from RF power to beam power during the beam acceleration, an 80-kW RF source should suffice. The beam power after acceleration is 120 kW. In the drift region, the spiral beam rotates about the axis with a frequency of 8 GHz and electrons perform cyclotron orbits about the focusing field with a gyration radius $R_g = 0.4$ cm. In the output interaction for a desired output frequency of 32 GHz, a TM_{410} mode cavity with a radius $b = 1.1$ cm is required. Under these conditions, from our numerical study in the previous section, an output cavity of suitable length L' should yield 100 kW of output power radiation at 32 GHz with an efficiency of 83 percent.

As shown in the MAGIC simulations [Figure 7(a)], on exiting the cavity, the spent beam remains nearly monoenergetic. This feature, with the help of an energy recovery scheme such as a depressed collector, should yet enhance the overall efficiency of the device. If an X-band klystron ($\eta_{klys} = 50\%$, $G_{klys} = 50$ dB) is employed as the driver for this device, the system (klystron-MFM) should provide a gain of $G_s = 50$ dB with an efficiency of 42 percent. Should a depressed collector with $\eta_c = 60$ percent be used, the system efficiency is increased to $\eta_s = 46$ percent. Table 1 lists the parameters for this point design.

Table 1. Ka-band MFM point design parameters.

Parameter	Units	Value
Input Frequency, $\omega/2\pi$	GHz	8
Input Cavity Radius, a	cm	2.2
Cavity Mode	—	TM_{110}
Input Power, P_{in}	kW	80
Initial Beam Energy	keV	50
Beam Current, I_o	A	1
Accel. Beam Energy	keV	120
Beam Gyroradius, R_g	cm	0.4
Output Frequency, $\omega_o/2\pi$	GHz	32
Output Cavity Mode	—	TM_{410}
Output Cavity Radius, b	cm	1.1
Output RF Power, P_o	kW	100
System Gain, G_s	dB	50
η_{klys}	percent	50
η_{rf}	percent	83
η_c	percent	60
η_s	percent	46

VIII. Conclusions

In this article, we have presented a new concept for generating high-power, high-frequency electromagnetic radiation. The MFM is a vacuum tube that employs a two-cavity system wherein an electron beam is modulated by the input cavity and where such a modulated beam excites high-power microwaves in the output cavity. The output cavity frequency is a multiple of the input frequency. Via analytical studies, we have shown the matching conditions necessary for successful beam acceleration in the input cavity and for frequency multiplication and energy transfer in the output cavity. We showed that 100 kW of 32-GHz radiation could be attained by using an 80-kW 8-GHz input signal. The resulting MFM could become a serious candidate as the high-power source of choice for future Ka-band radar and communications transmitters.

References

[1] J. E. Velazco, "Study of Rotating-Wave Electromagnetic Modes for Applications in Space Exploration," *The Interplanetary Network Progress Report*, vol. 42-206, Jet Propulsion Laboratory, Pasadena, California, pp. 1–16, August 15, 2016.
http://ipnpr.jpl.nasa.gov/progress_report/42-206/206A.pdf

[2] J. Velazco and P. Ceperley, "A Discussion of Rotating Wave Fields for Microwave Applications," *IEEE Transactions on Microwave Theory and Techniques*, vol. 41, no. 2, February 1993.
https://dx.doi.org/10.1109/22.216476

[3] J. E. Velazco, "Study of Compact Rotating-Wave Accelerators for Medical and Industrial Applications" (Invited Paper), *Proceedings of the Fourteenth International Conference on the Applications of Accelerators In Research and Industry*, DE5, University of North Texas, Denton, Texas, November 6–9, 1996.
https://dx.doi.org/10.1063/1.52415

[4] J. E. Velazco, M. Taylor, Y. Liu, R. Hodyss, and A. Allwood, "A Novel Rotating-Wave X-Ray Source for Analysis of the Martian Landscape," *The Interplanetary Network Progress Report*, vol. 42-207, Jet Propulsion Laboratory, Pasadena, California, November 15, 2016.
http://ipnpr.jpl.nasa.gov/progress_report/42-207/207B.pdf

[5] J. Velazco, W. M. Black, T. Godlove, and F. Mako, "The Design of a Deflection Cavity for a New Microwave Amplifier," *Proceedings of IEEE Southeastcon Conference*, May 1990.

[6] M. W. Black, J. E. Velazco, T. F. Godlove, and F. Mako, "Transverse-Modulation Klystron Design Considerations and Preliminary Results," *Proceedings of IEEE International Electron Devices Meeting*, December 8, 1991.

[7] J. E. Velazco and F. M. Mako, "Limited Spatial Region for Beam-Wave Synchronous Interactions in Rotating Mode Resonators," *Applied Physics Letters*, vol. 63, no. 22, pp. 3087–3089, November 29, 1993.
https://dx.doi.org/10.1063/1.110241

[8] P. H. Ceperley and J. E. Velazco, "Tuning a Rotating Mode Resonator," *Review of Scientific Instruments*, vol. 66, no. 1, pp. 256–260, January 1995.